COMPDYN 2013
4th ECCOMAS Thematic Conference on
Computational Methods in Structural Dynamics and Earthquake Engineering
M. Papadrakakis, V. Papadopoulos, V. Plevris (eds.)
Kos Island, Greece, 12–14 June 2013

ASSESSMENT OF BOUNDARY CONDITIONS FOR DAM-RESERVOIR INTERACTION PROBLEMS

Loizos Pelecanos[1], **Stavroula Kontoe**[1], **Lidija Zdravković**[1]

[1]Department of Civil & Environmental Engineering, Imperial College, London SW7 2AZ
e-mail: loizos.pelecanos05@imperial.ac.uk, stavroula.kontoe@imperial.ac.uk,
l.zdravkovic@imperial.ac.uk

Keywords: boundary conditions, hydrodynamic pressures, dams, solid finite elements, reservoir, dynamic analysis

Abstract. *This paper investigates four different boundary conditions for the upstream reservoir boundary for dam-reservoir interaction problems. Accurate numerical modelling of the reservoir hydrodynamic pressures on dams is used as a means of assessment of the different boundary conditions. The reservoir is modelled with two-dimensional plane-strain displacement-based isoparametric solid finite elements. The study considers stiff dams with vertical upstream faces under ramp and harmonic acceleration loads. The numerical results were compared and found to be in good agreement with available closed-form solutions. The same approach may be used in analyses of other waterfront structures such as quay walls.*

1 INTRODUCTION

The seismic behaviour of dams has long been studied [11] and several methods of analysis were developed such as the pseudo-static [26] [23], the shear beam [1] and the dynamic finite element [2, 3] methods. Significant progress was made regarding the dynamic characteristics of inhomogeneous visco-elastic dams [7, 8] and the seismic response of nonlinear elasto-plastic dams [10]. However, most of the analyses neglect the hydrodynamic pressures from the upstream reservoir and consider only the hydrostatic part of the reservoir pressures.

The hydrodynamic pressures on dams during earthquakes were first investigated by Westergaard [29] who considered a stiff dam with a vertical upstream face under harmonic loading. Zangar [32] [33] and Chwang [6] considered dams with a sloped upstream face whereas Liu [18] considered a sloped reservoir base. Moreover, the effects of the reservoir water compressibility were studied by Chopra [4] who showed that the magnitude of the total hydrodynamic force on the dam from a compressible reservoir depends on the frequency of the applied loading. In addition, the work of Chopra [4] was extended to investigate the hydrodynamic pressures due to general (non-harmonic) acceleration loading and a closed-form solution was developed.

A number of analytical solutions were developed [29] [33] [4] covering several aspects of the problem (such as slope angle, water compressibility, nature of load etc.) and provided various solutions for the magnitude and distribution of the hydrodynamic pressures on dams. However, they suffered from several assumptions and limitations (such as simple geometries, undeformable dams etc.). More elaborate problems involving complicated geometries, deformable and inhomogeneous dams required discretisation of the reservoir domain [12], so that reservoir-dam interaction can be fully analysed. To model the reservoir, various techniques have been developed, such as Eulerian [22] and Lagrangian [30] fluid finite elements, boundary elements [28] etc. However, all these advanced approaches that model the reservoir domain require appropriate boundary conditions at the truncated upstream boundary of the reservoir.

This paper investigates the numerical modelling of the hydrodynamic pressures by discretising the reservoir domain. The main aim is to assess different boundary conditions employed on the upstream reservoir boundary and their effect on the hydrodynamic pressures on the dam face. The reservoir is modelled with two-dimensional plane-strain displacement-based isoparametric quadrilateral solid finite elements (FEs) which are the same as those used to model the dam structure. The investigation considers the upstream reservoir boundary condition (BC), its distance from the dam and also the dam-reservoir and foundation-reservoir interfaces under two types of acceleration loading. Additionally, the geometric (element discretisation) and material (water compressibility) properties of the reservoir domain on the performance of the considered boundary conditions are discussed.

2 STATEMENT OF THE PROBLEM

The problem under study is shown schematically in Figure 1. It consists of a dam (1) which retains a large volume of water in the reservoir (2) and rests on the ground (3) which serves as the foundation of the dam. Under seismic or general dynamic conditions, the reservoir induces hydrodynamic pressures on the upstream (US) dam face, A-B. The hydrodynamic pressures induced on the dam depend on the magnitude and the frequency characteristics of the load as well as the properties of the dam, the foundation and the reservoir.

In order to model efficiently and economically the hydrodynamic pressures, the US reservoir is truncated at some distance from the dam, (C-D). Likewise, the foundation soil is truncated at some distance from the dam and the reservoir (E-F-G-C). On both soil and reservoir boundaries,

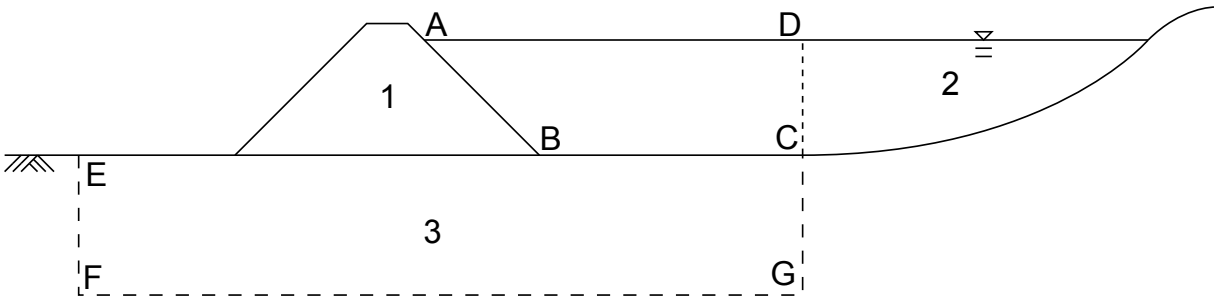

Figure 1: Geometry of the dam-reservoir-foundation system: (1) dam, (2) reservoir, (3) foundation soil, US dam face A-B, US reservoir boundary C-D and foundation boundary E-F-G-C.

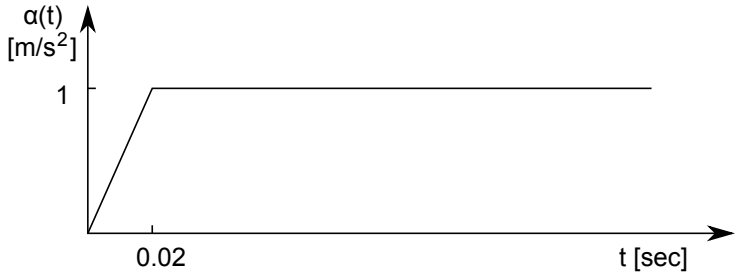

Figure 2: The ramp acceleration load used by Küçükarslan et al. [16]

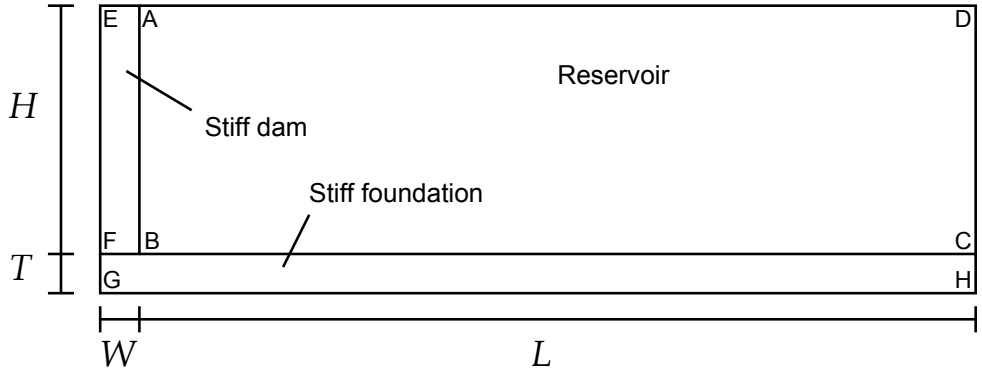

Figure 3: Geometry of the dam-reservoir system considered

special absorbing boundary conditions (BCs) need to be applied so that reflection of outgoing waves is avoided.

Therefore, issues that need to be considered for appropriate modelling of the hydrodynamic pressures include: the type of the absorbing BC on the upstream reservoir boundary (C-D), the distance of this BC (B-C), the dam-reservoir and foundation-reservoir interfaces (A-B-C) and the geometric and material properties of the reservoir (A-B-C-D).

3 RAMP ACCELERATION

This section concentrates on the evaluation of the hydrodynamic pressures on a stiff (undeformable) dam with a vertical upstream face under a ramp acceleration load. The modelling of hydrodynamic pressures on dams was recently investigated by Küçükarslan et al. [16] who represented the reservoir in their analyses with Eulerian fluid elements. Their study considered a stiff dam with a vertical upstream face of height H=180m, following the work of Tsai et al. [27], and examined the evolution of hydrodynamic pressures at the base of the dam (Point B in Figure 1) with time, under the ramp acceleration load shown in Figure 2.

3.1 Upstream boundary condition

Following the work of Küçükarslan et al. [16], analyses were carried out using the dam-reservoir system shown in Figure 3 under the above-mentioned ramp acceleration, modelling the reservoir with solid elements. All the analyses carried out were two-dimensional plane-strain dynamic in the time-domain using the FE software ICFEP (Imperial College Finite Element Program) [21]. The time-integration scheme employed was the generalised α-method of Chung & Hulbert [5] implemented in ICFEP by Kontoe et al. [14] and the time step used was Δt = 0.002sec.

In Figure 3, A-B-F-E represents a stiff dam with a vertical upstream face (A-B), A-B-C-D represents the reservoir and F-C-H-G represents a stiff rock underneath the reservoir. The height of the reservoir was H=180m, whereas five values were adopted for the length of the reservoir, L=540, 960, 1260, 1800 and 2400m (i.e. L/H = 3, 5.33, 7, 10 and 13.33). The width of the stiff dam, W and the thickness of the foundation, T were 18m. The maximum element dimension, d used was 4.5m (= H/40). The load was applied as prescribed values of acceleration in the horizontal direction along the bottom and left vertical boundaries, while the displacements in the vertical direction were restricted to be equal to zero. Four boundary conditions (BCs) were considered for the upstream reservoir boundary (CD):

- Free, i.e. zero stress and displacement in the horizontal and vertical directions respectively
- Viscous [19], i.e. dashpots in the horizontal and zero displacements in the vertical direction
- Cone [13], i.e. dashpots and springs in the horizontal and zero displacements in the vertical direction
- Viscous with a constant hydrostatic pressure

As far as the last BC is concerned, it should be noted that, according to Parrinello & Borino [20] (who followed the Lagrangian approach to discretise the reservoir domain), the Sommerfeld radiation condition [24] [25] may be represented by a series of dashpots and a hydrostatic stress at the boundary.

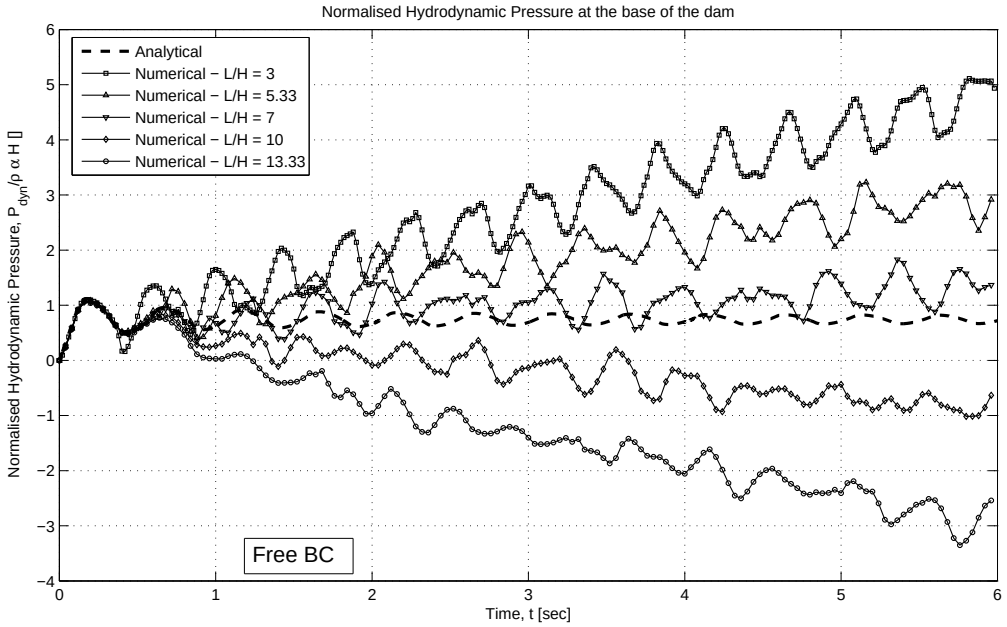

Figure 4: Hydrodynamic pressures at the base of the dam due to the ramp acceleration for the Free BC

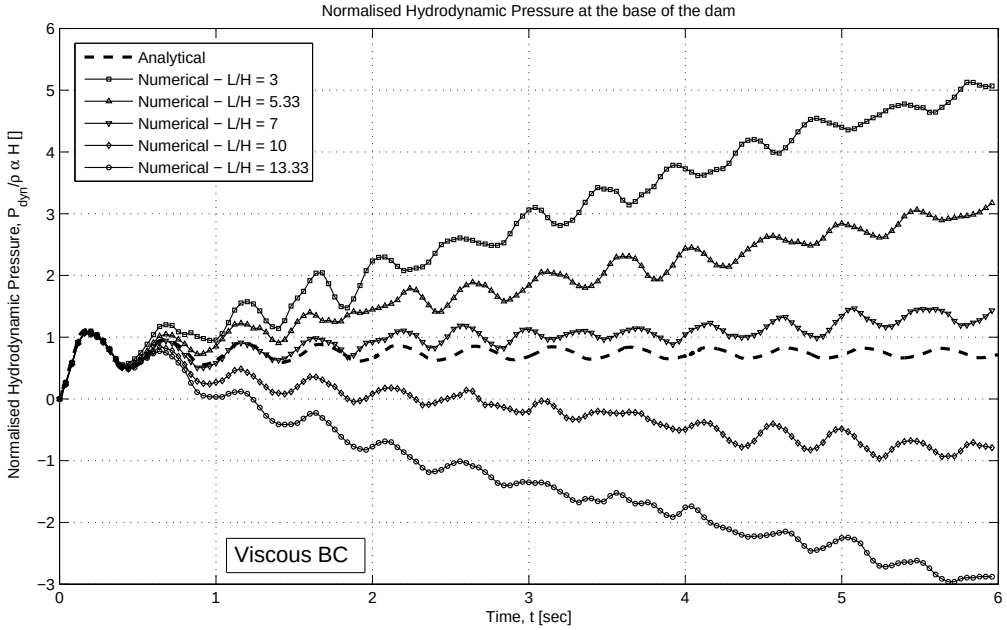

Figure 5: Hydrodynamic pressures at the base of the dam due to the ramp acceleration for the Viscous BC

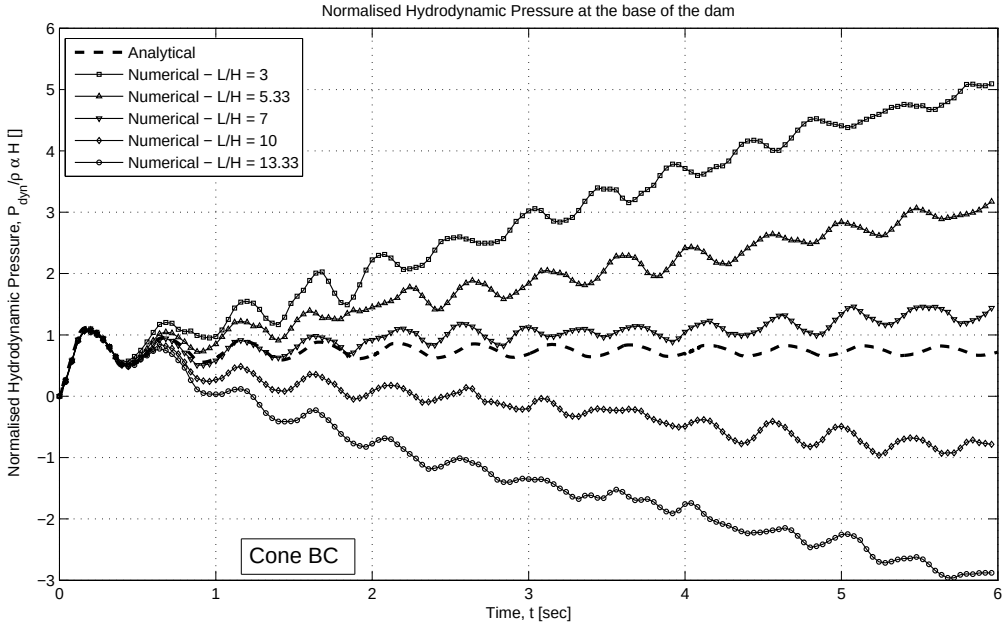

Figure 6: Hydrodynamic pressures at the base of the dam due to the ramp acceleration for the Cone BC

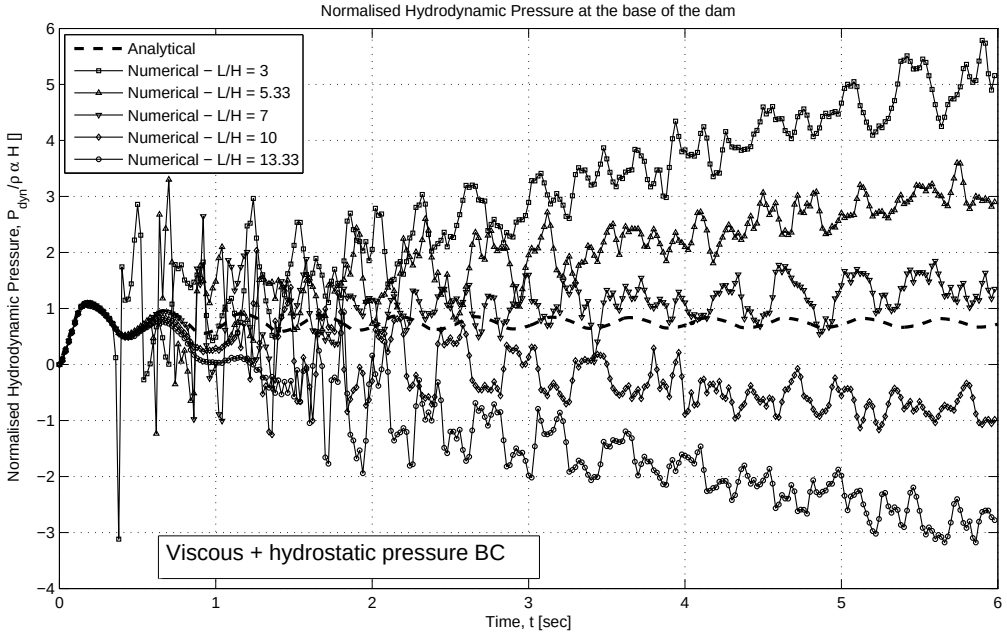

Figure 7: Hydrodynamic pressures at the base of the dam due to the ramp acceleration for the Viscous + hydrostatic stress BC

The reservoir water is modelled as a linear elastic material and its properties are the bulk modulus, $K_w = 2.2 \cdot 10^6$ kPa and the shear modulus, $G_w = 100$ kPa. A nominal value of the shear modulus was adopted to avoid numerical instability without causing unrealistic shear wave propagation in the water. The dam and foundation (A-B-C-H-G-F-E in Figure 3) were considered as rigid, therefore the bulk modulus assigned was $K_d = 10^8 \cdot K_w = 2.2 \cdot 10^{14}$ kPa. No material damping was specified in the reservoir, dam or foundation domains. The dashpots and the springs are defined by Equations 1 and 2 respectively.

$$\sigma = \rho V_p \dot{u} \tag{1}$$

$$\sigma = \rho \frac{V_p^2}{2r} \dot{u} \tag{2}$$

where σ is a normal stress on the boundary, ρ is the density of the material the BC has been applied to (i.e. water in this case), V_p is the p-wave velocity of the water (=1483 m/s), r is the distance of the boundary from the excitation source (taken as equal to the length, L of the reservoir) and $\dot{u}$ is the velocity in the horizontal direction. More details about these BCs may be found in Kontoe et al. [15].

Figures 4 - 7 show the hydrodynamic pressure at the base of the dam (Point B) with time for the four different BCs considered. The hydrodynamic pressures, P_{dyn}, are normalised with respect to $\rho a H$, where ρ is the mass density of water, $a = 1\text{m/s}^2$ is the maximum value of the ramp acceleration load (see Figure 2) and H is the height of the reservoir. The numerical results are compared to the analytical solution which was calculated using the relation of Chopra [4], given by Equation 3.

$$p(y,t) = \frac{4\gamma_w V_p}{\pi g} \sum_{n=1}^{+\infty} \frac{(-1)^{n-1}}{2n-1} \cos(\lambda_n y) \int_0^t \ddot{u}_g(\tau) J_o[\lambda_n V_p (t-\tau)] d\tau \tag{3}$$

where, y is the vertical distance from the base of the dam, t is the time, γ_w is the unit weight of water, V_p is the p-wave velocity of water, λ_n is the n^{th} wavelength, $\ddot{u}_g(t)$ is the ground acceleration and $J_o(\cdot)$ is a Bessel Function of the first kind of order 0.

As it may be observed from Figures 4 - 7, none of the four BCs satisfactorily captured the analytical solution for the hydrodynamic pressures, regardless of the L/H ratio. In all four cases the first half cycle is predicted correctly, whereas the hydrodynamic pressures are generally increasing or decreasing with time for shorter and longer meshes respectively. Moreover, the amplitude of the pressure fluctuations for the Free BC is significantly larger than that of the pressures from the analytical solution. The amplitude of the fluctuations for both the Viscous and the Cone BCs is more comparable to the analytical solution. The results for the Viscous + hydrostatic pressure BC show some spurious peak values of the pressure which occur at different times according to the length of the mesh. The longer the FE mesh, the later the peaks appear. This is believed to be due to the specification of a constant stress at the boundary which causes reflection of the waves back towards the dam.

3.2 Reservoir-dam and reservoir-foundation interface

The analyses were repeated after the introduction of zero-thickness isoparametric interface elements [9] [21] at the reservoir-dam and reservoir-foundation interfaces (ABC in Figure 3). The reason for introducing these elements is to allow relative movement between the reservoir

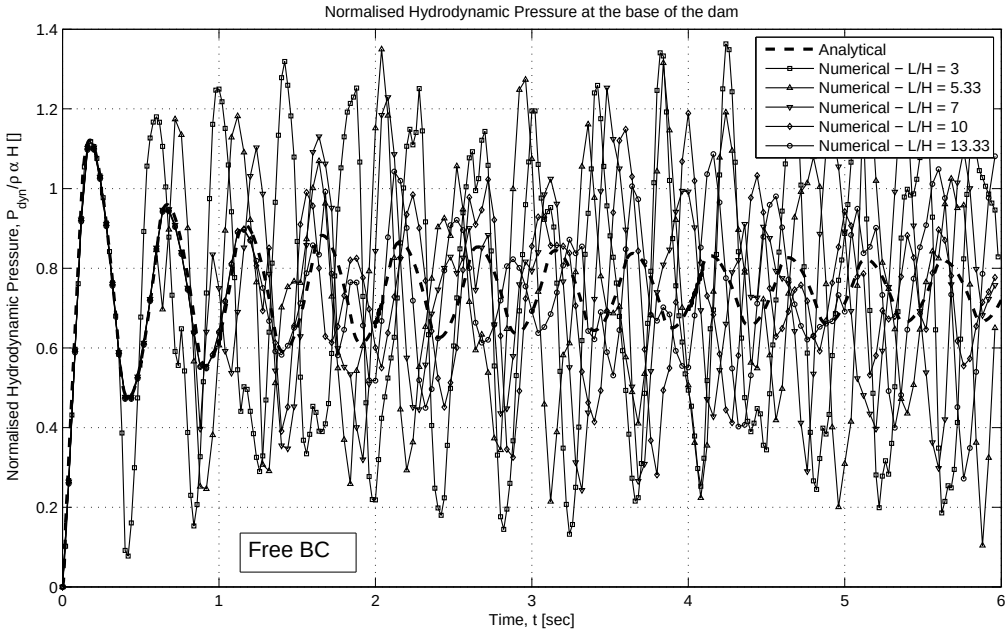

Figure 8: Hydrodynamic pressures at the base of the dam due to the ramp acceleration for the Free BC with interface elements

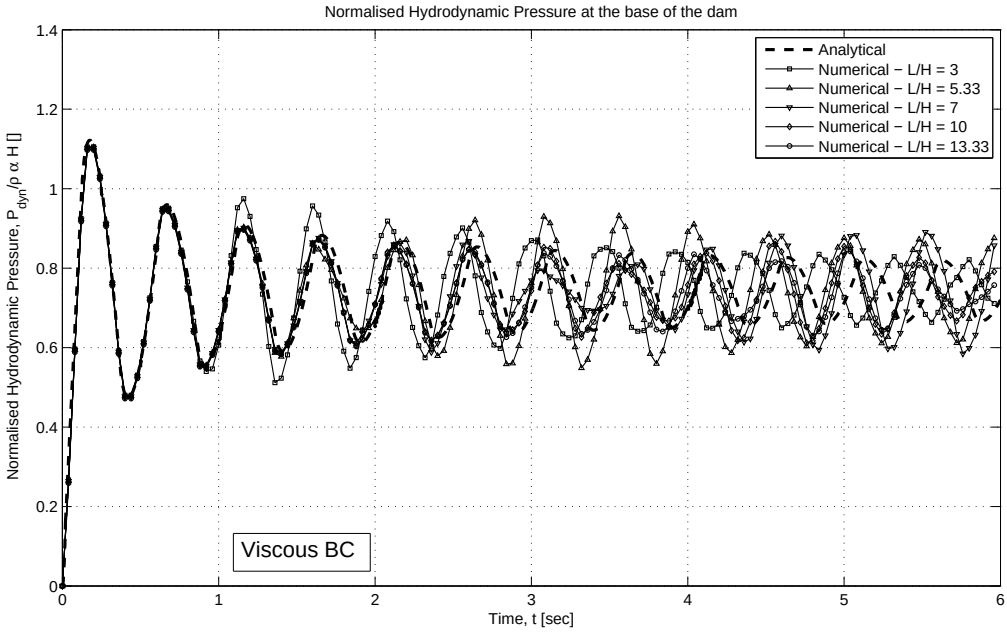

Figure 9: Hydrodynamic pressures at the base of the dam due to the ramp acceleration for the Viscous BC with interface elements

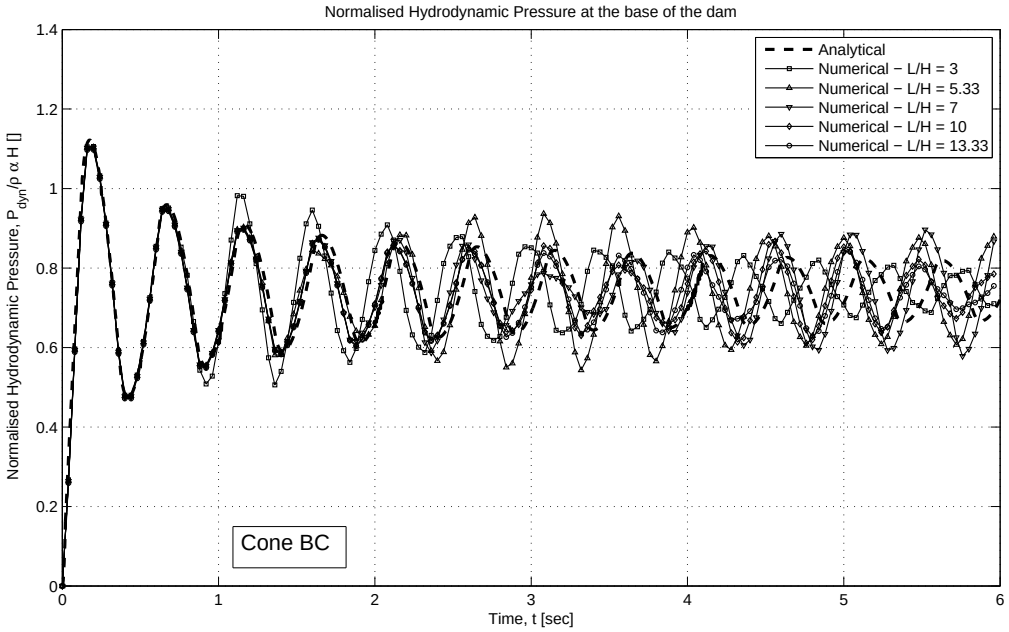

Figure 10: Hydrodynamic pressures at the base of the dam due to the ramp acceleration for the Cone BC with interface elements

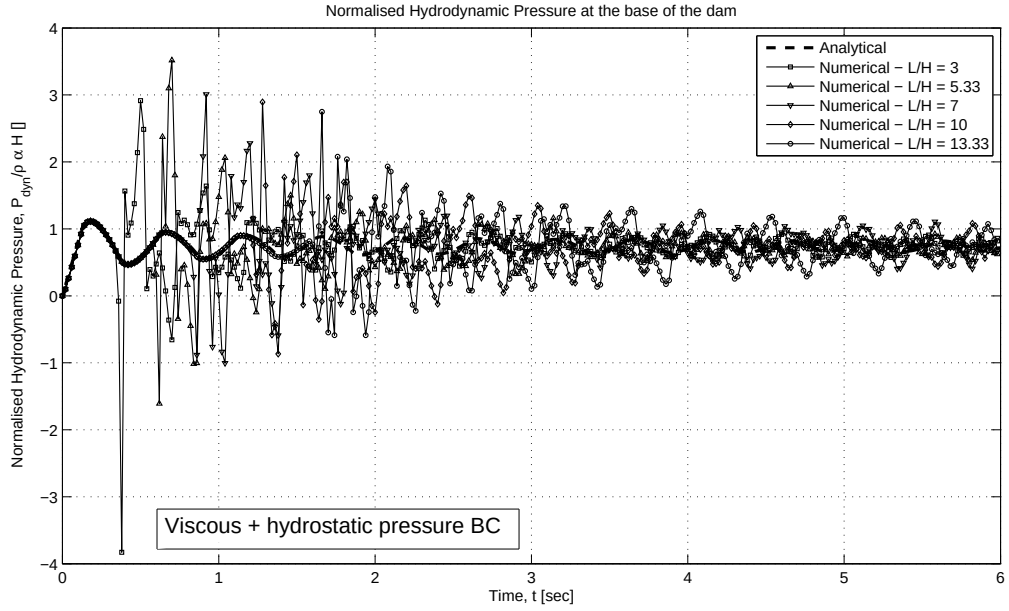

Figure 11: Hydrodynamic pressures at the base of the dam due to the ramp acceleration for the Viscous + hydrostatic stress BC with interface elements

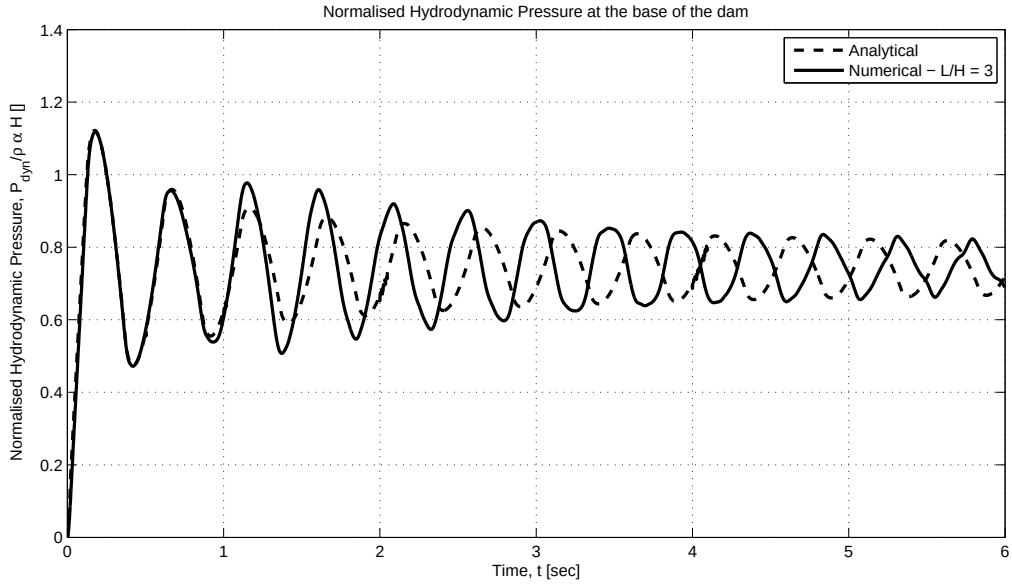

Figure 12: Hydrodynamic pressures at the base of the dam due to the ramp acceleration with the Viscous BC for $L/H = 3$

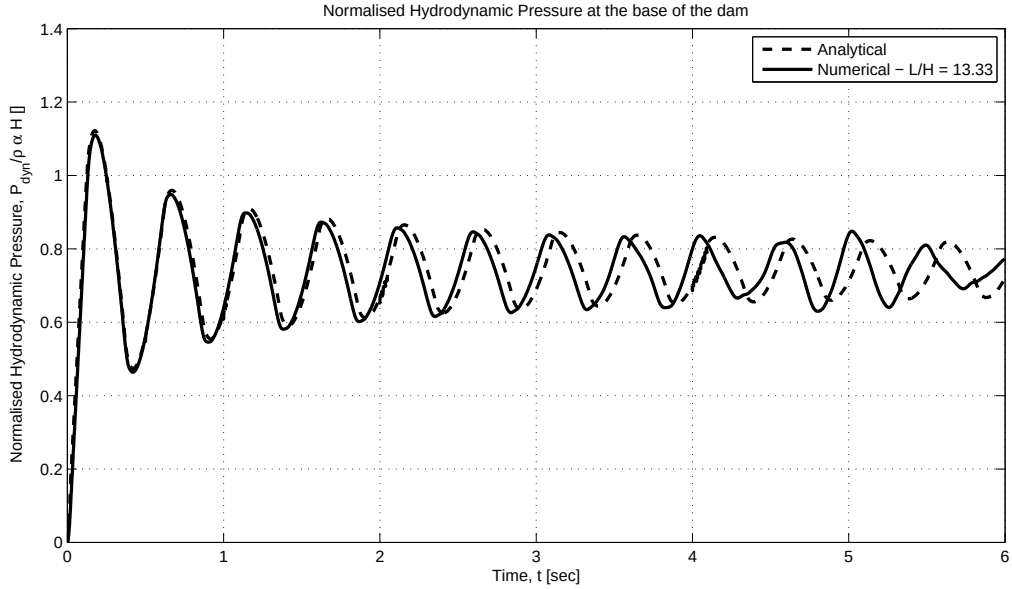

Figure 13: Hydrodynamic pressures at the base of the dam due to the ramp acceleration with the Viscous BC for $L/H = 13.33$

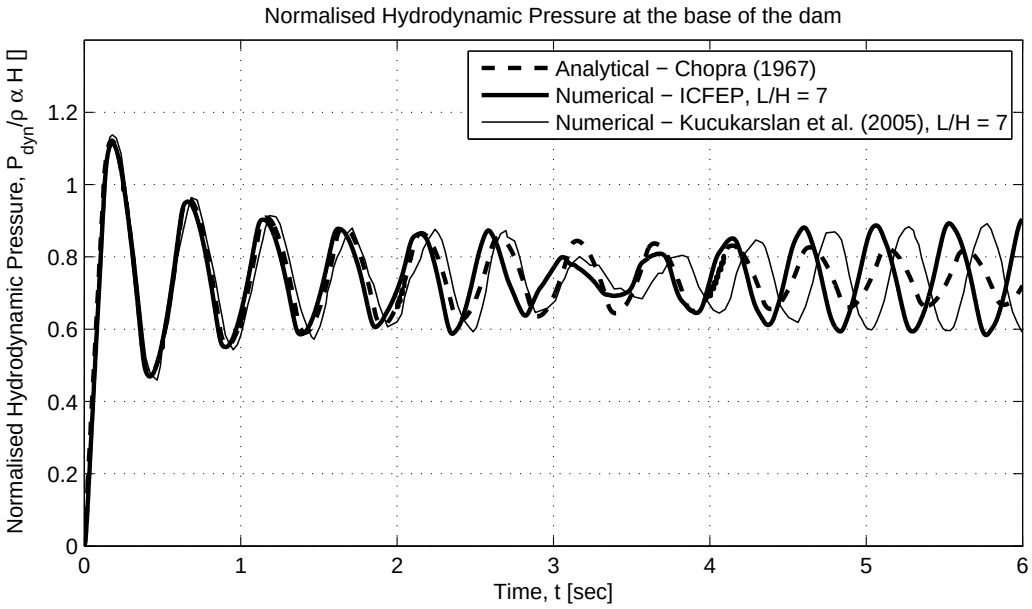

Figure 14: Comparison of the hydrodynamic pressures at the base of the dam due to the ramp acceleration with the Viscous BC for $L/H = 7$ against the analytical solution of Chopra [4] and the numerical results of Küçükarslan et al. [16].

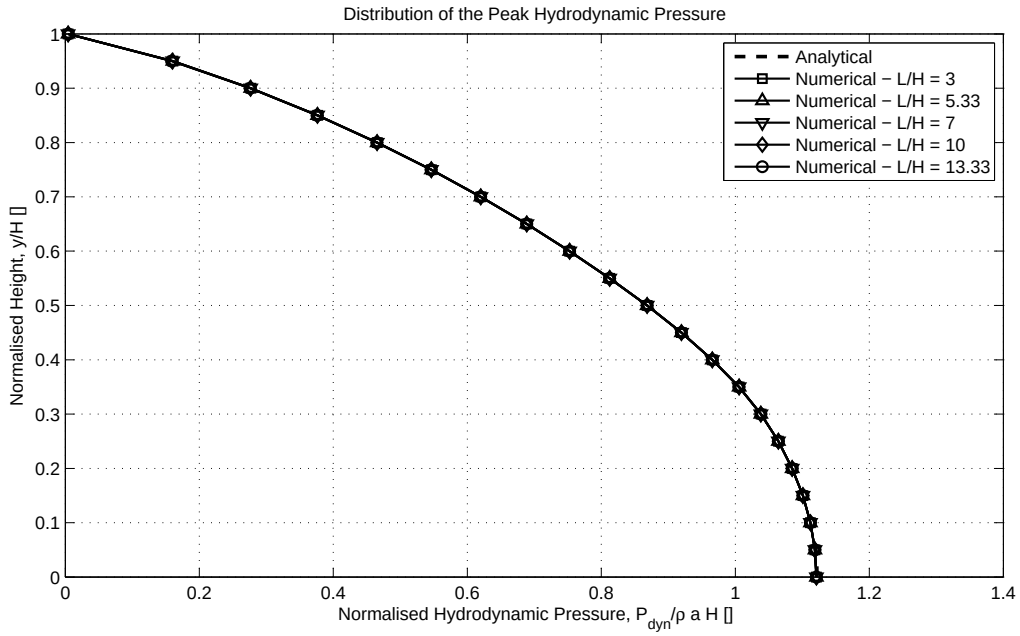

Figure 15: Distribution of the peak hydrodynamic pressure on the face of the dam due to the ramp acceleration for the Viscous BC

and the solid material. For this reason, a very high normal and very low shear stiffness were assigned to these elements so that only shear relative movement occurs.

Figures 8 - 11 show the evolution of the hydrodynamic pressures at the base of the dam (Point B) with time for the all four BCs. As it may be observed, the results are now in better agreement with the analytical solution as the general increase or decrease of the pressures with time disappeared. However, the amplitude of the fluctuations for the Free BC (Figure 8) is still larger than that of the analytical solution and the pressures for the Viscous + hydrostatic pressure BC (Figure 11) still show some spurious peaks. As far as the Viscous (Figure 9) and the Cone (Figure 10) BCs are concerned, a good agreement is obtained although there are still some differences and these are mainly a slight increase of the amplitude and a small shortening of the period of the pressure fluctuations, which seem to be more severe for the shorter FE meshes.

Moreover, Figures 12 and 13 show the comparison between the analytical and the numerical (with the Viscous BC) hydrodynamic pressure time-histories at the base of the dam for $L/H = 3$ and 13.33 respectively. It is shown that for the shorter mesh, the increase in the amplitude of the pressure fluctuations occurs much earlier than that for the longer mesh and also the shortening of the period is more pronounced. Figure 14 compares the computed hydrodynamic pressures for $L/H = 7$ with both the analytical solution and the numerical solution of Küçükarslan et al. [16] (obtained by adopting the Eulerian approach). It is shown that the agreement of both numerical approaches (Eulerian fluid FEs and elastic solid FEs) with the analytical approach of Chopra is acceptable. Finally, Figure 15 compares the distribution of the peak hydrodynamic pressure on the upstream face of the dam for all 5 lengths computed with the Viscous BC with the analytical solution, showing an excellent agreement (as it occurs during the first half cycle). It should be noted that the results for the case of the Cone BC with interface elements are almost identical to the results of the Viscous BC and are not shown here for brevity.

Of course, the ramp acceleration may not be the most suitable load to determine an appropriate length of the reservoir and consequently the distance of the boundary from the problem of interest. However, so far it may be concluded that the Viscous and the Cone BCs perform well as absorbing BCs on the reservoir and that interface elements with appropriate stiffness should be placed at the interface between the reservoir and the solid domains (dam and foundation). It is therefore concluded that both the "Free" and "Viscous + hydrostatic pressure" BCs are not appropriate absorbing BCs and will not be considered further in this study.

4 HARMONIC ACCELERATION

4.1 Frequency Response

As mentioned earlier, Chopra [4] investigated the hydrodynamic pressures on dams under harmonic loading and expressed the results in terms of a spectrum of forces. In order to examine the performance of the Viscous and Cone BCs under a wide range of loading frequencies, the same analyses were repeated for different loading frequencies according to Equation 4, with amplitude $a_0 = 1$ m/s^2 for 40 cycles.

$$a(t) = a_0 \cos \omega t \tag{4}$$

where, $a(t)$ is acceleration, a_0 is the amplitude of the harmonic acceleration, ω is the circular frequency of the load and t is time. The time step used was Δt = T/40, where T = $2\pi/\omega$.

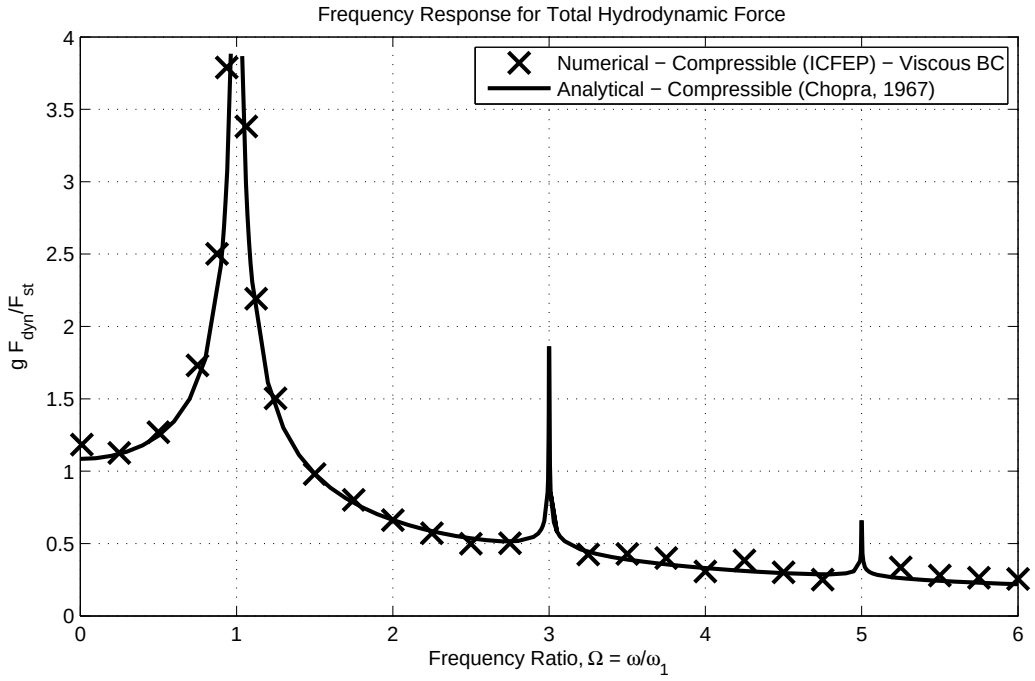

Figure 16: Frequency response of the total hydrodynamic induced by a compressible reservoir due to horizontal harmonic loading with the Viscous BC

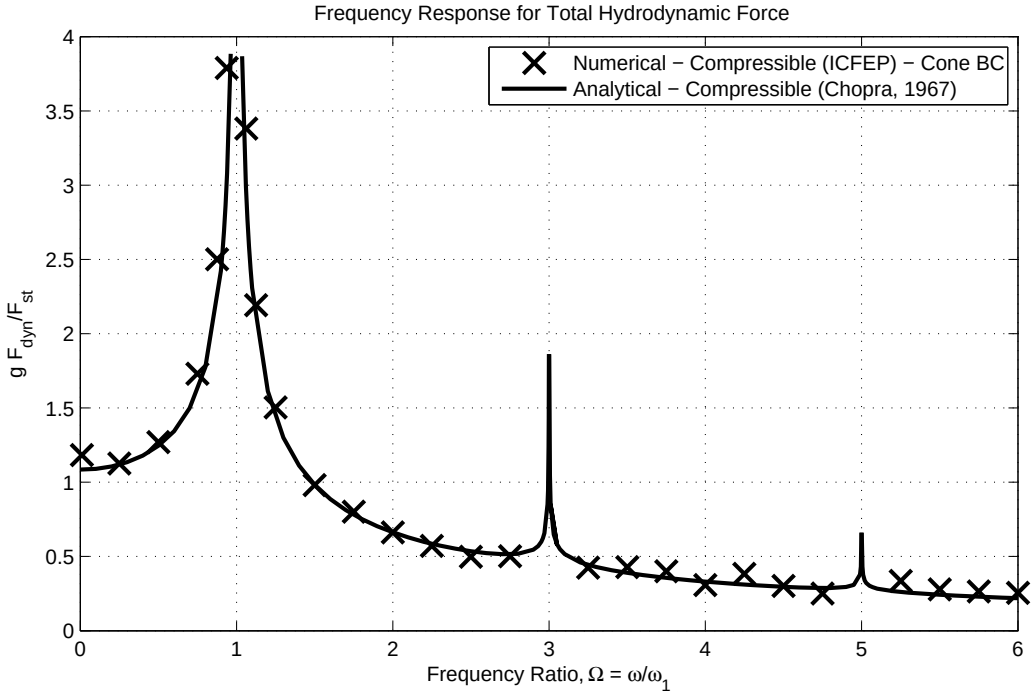

Figure 17: Frequency response of the total hydrodynamic induced by a compressible reservoir due to horizontal harmonic loading with the Cone BC

Figures 16 and 17 show the ratio of the total hydrodynamic force, F_{dyn} (hydrodynamic pressures integrated over the upstream dam face at steady state conditions), over the hydrostatic force, F_{st}, multiplied by the acceleration of gravity, g, against the frequency ratio, $\Omega = \omega/\omega_1$ for the Viscous and Cone BCs respectively. The parameter ω refers to the circular frequency of the load and ω_1 to the fundamental circular frequency of the reservoir, given by Equation 5 [4]. The values of the ratio $g \cdot F_{dyn}/F_{st}$ at the natural frequencies of the reservoir ($\omega/\omega_1 = 1$, 3, 5, ...) are not included as the hydrodynamic pressures, F_{dyn}, from the reservoir become infinite due to resonance.

$$\omega_1 = \frac{\pi V_p}{2H} \tag{5}$$

where H is the height of the reservoir and V_p is the p-wave velocity of water.

As it may be observed, a generally good agreement is obtained for the whole spectrum of frequencies for both BCs (Viscous and Cone) and in fact their performance is almost identical. This suggests that both of these BCs can be applied on the upstream boundary of the reservoir in order to model the hydrodynamic pressures on dams due to a dynamic load of a wide range of frequencies.

4.2 Water compressibility

The significance of considering the true compressibility of water was highlighted by Chopra [4]. In order to examine the behaviour of the numerical model (BCs) if water is considered incompressible, the analyses of the previous section with the Viscous BC were repeated for the same loading frequencies. The compressibility of the water, K_w was taken as 100000 times the real value (i.e. $K_w = 2.2 \cdot 10^{11}$ kPa). The resulting force spectrum is shown in Figure 18.

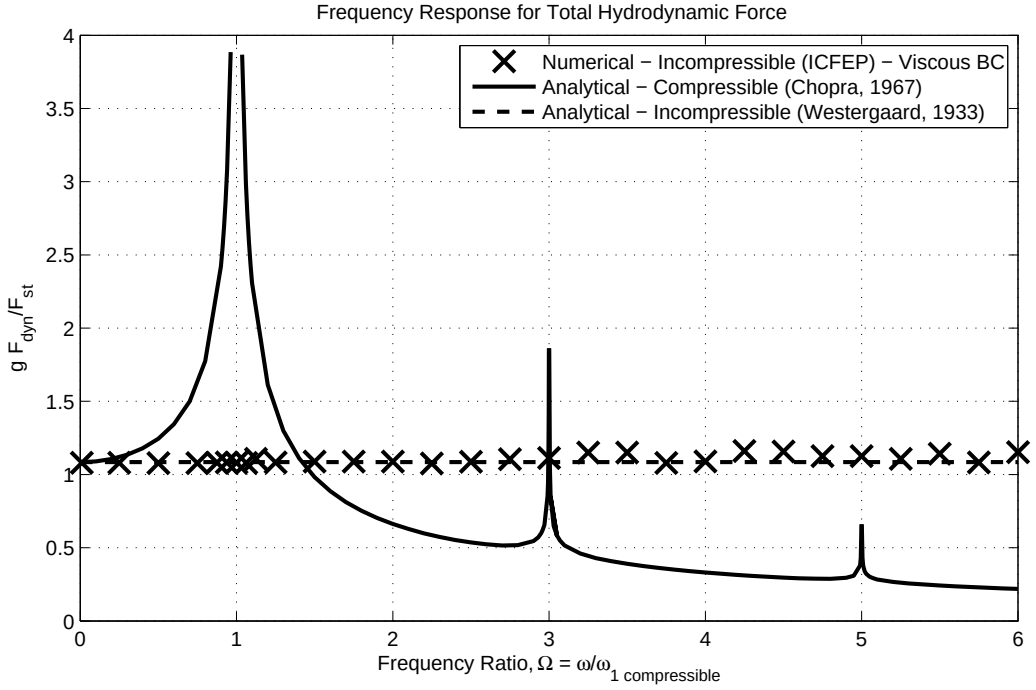

Figure 18: Frequency response of the total hydrodynamic induced by an incompressible reservoir due to horizontal harmonic loading

The numerical results for incompressible water agree with the analytical result of Westergaard [29] (Equation 6), which was also confirmed by Chopra [4]. The higher hydrodynamic pressures due to resonance for loading frequencies close to the natural frequency of the reservoir cannot be predicted, whereas the pressures for higher frequency loads are overestimated. It is therefore suggested that water compressibility should be taken into account by using the real value of bulk modulus of the water, K_w in order not to underestimate or overestimate the pressures for different loading frequencies.

$$\frac{g \cdot F_{dyn}}{F_{st}} = \frac{g \cdot 0.543(a_0/g)\gamma_w H^2}{1/2\gamma_w H^2} = 1.09 \tag{6}$$

4.3 Effect of element size

A further investigation was carried out in order to examine the effect of the size of the reservoir elements on the hydrodynamic pressures. When modelling dynamic problems, care needs to be taken in order to appropriately model wave propagation and therefore a sufficient number of nodes should be provided to model the length of the propagating wave [19] [17]. A very fine mesh could in one hand provide sufficient nodes; on the other hand, it would increase the computational cost. The aim is therefore to identify the largest element size that provides accurate results.

For this investigation, a FE mesh of height, H=90m and length, L=900m was employed. Eight-noded isoparametric quadrilateral elements [21] were used as shown in Figure 19. The Viscous BC was applied on the upstream reservoir boundary. The harmonic load is described by Equation 4 with a single value of ω so that the ratio $\omega/\omega_1 = 4$. The various element sizes used are listed in Table 1 and are expressed as a fraction of the wavelength, λ. For a monochromatic load (i.e. single frequency, $f = \omega/2\pi$), the wavelength of a p-wave (with velocity, V_p) is given by Equation 7.

$$\lambda = \frac{V_p}{f} \tag{7}$$

Considering the fundamental frequency of vibration of a reservoir, $f_1 = \omega_1/2\pi$ (ω_1 from Equation 5), then the wavelength is given by Equation 8.

$$\lambda = \frac{4H}{f/f_1} = \frac{4H}{\omega/\omega_1} \tag{8}$$

Figure 20 shows the distribution of the peak hydrodynamic pressure on the upstream face of the dam for all 11 values of the element dimension, d. The results from the finest mesh ($\lambda/d = 20$) are considered to be the most accurate because a large number of nodes has been provided to model the wavelength. As it may be observed from that figure, the peak hydrodynamic pressure obtained using elements of size equal or smaller than a fifth of the wavelength deviate significantly from the most accurate prediction, whereas the results for an element dimension equal to a sixth and an eighth of the wavelength are close. It is therefore suggested that if the reservoir is modelled with eight-noded quadrilateral solid elements, the side of these elements should be smaller than a fifth of the wavelength.

5 CONCLUSIONS

Four boundary conditions for the upstream reservoir boundary for dam-reservoir interaction problems were explored. The study focussed on the influence of this boundary condition on the

Table 1: Size of the reservoir finite elements considered

CASE	**Element size, d [m]**	$H/d = \lambda/d$
1	90	1
2	45	2
3	30	3
4	22.5	4
5	18	5
6	15	6
7	11.25	8
8	9	10
9	7.5	12
10	6	15
11	4.5	20

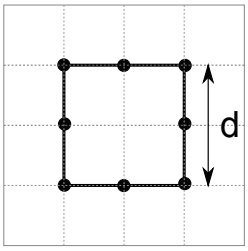

Figure 19: Eight-noded isoparametric quadrilateral element [21]

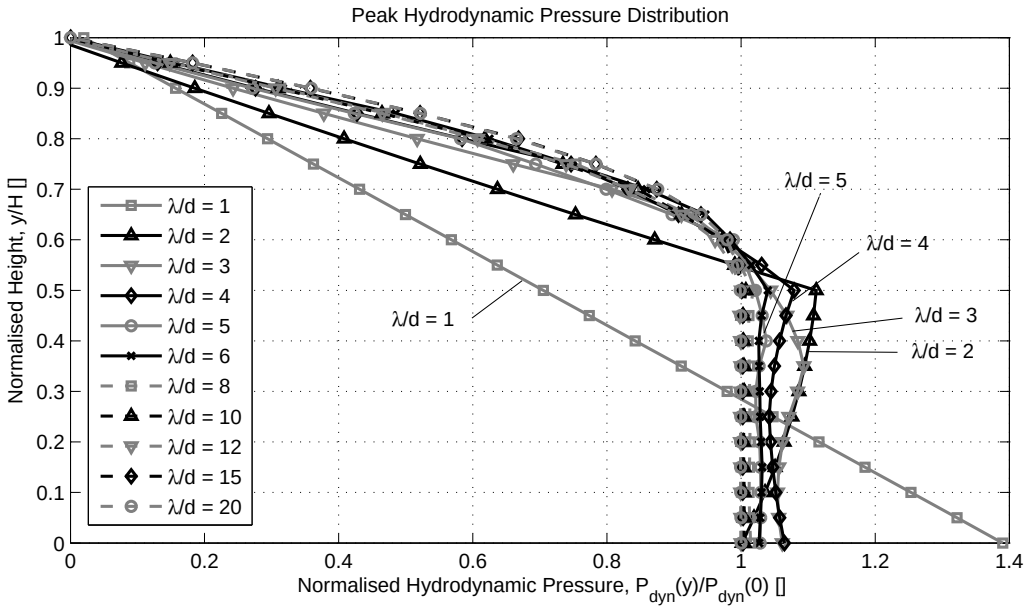

Figure 20: Distribution of the peak hydrodynamic pressure on the dam face for different element sizes

modelling of the hydrodynamic pressures on dams. The reservoir domain was discretised with displacement-based isoparametric solid finite elements. Stiff dams with vertical upstream faces were investigated under ramp and harmonic acceleration loads. In addition, the effect of the geometric (element discretisation) and material (water compressibility) properties of the reservoir domain on the performance of the considered boundary conditions were examined. The results (hydrodynamic pressures and forces) have been compared to analytical solutions where available and showed a good agreement. The same approach may be used in analyses of other waterfront structures such as quay walls. The conclusions of this study may be summarised as follows:

- The Viscous and Cone BCs can be employed on the truncated upstream boundary of the reservoir to absorb the radiating waves. Their performance under ramp and a wide range of harmonic loading frequencies has been confirmed and it is almost identical. The Free and Viscous + hydrostatic pressures BCs were also examined and did not perform satisfactorily.
- At the interface between the reservoir and the dam and the reservoir and the foundation, interface elements should be used in order to allow relative movement between the water and the solid materials. Appropriate values should be used for the shear and normal stiffness of these elements.
- The reservoir water should not be treated as incompressible in order not to underestimate possible resonance for loading frequencies close to the fundamental frequencies of the reservoir and not to overestimate pressures for higher frequency loads.
- The size of the reservoir elements should be smaller than a fifth of the acoustic (p-wave) wavelength of the water.

ACKNOWLEDGEMENTS

The first author would like to express his acknowledgements to the Engineering and Physical Sciences Research Council (EPSRC), UK for the award of a Research Studentship.

REFERENCES

[1] Ambraseys, N. N., 1960, On the shear response of a two-dimensional truncated wedge subjected to arbitrary disturbance, Bull. Seism. Soc. Am., 50, 1, 45-56.

[2] Chopra, A. K., 1966, Earthquake effects on dams, PhD Thesis, University of California, Berkeley.

[3] Chopra, A. K., 1967, Earthquake response of earth dams, J. Soil Mech. Found. Div., ASCE, 93, SM2, 1399-1412.

[4] Chopra, A. K., 1967, Hydrodynamic pressures on dams during earthquakes, J. Engrg. Mech. Div., ASCE, 93, EM6, 205-223.

[5] Chung, J., Hulbert, G. M., 1993, A time integration algorithm for structural dynamics with improved numerical dissipation: the generalised-α method, J. Appl. Mech., 60, 371-375.

[6] Chwang, A. T., 1978, Hydrodynamic pressures on sloping dams during earthquakes. Part 2: Exact theory, J. Fluid Mech., 87, 2, 343-348.

[7] Dakoulas, P., Gazetas, G., 1985, A class of inhomogeneous shear models for seismic response of dams and embankments, Soil Dyn. and Earthq. Engrg., 4, 4, 166-182.

[8] Dakoulas, P., Gazetas, G., 1987, Vibration characteristics of dams in narrow canyons, J. Geotech. Engrg. Div., ASCE, 113, 8, 899-904.

[9] Day, R. A., Potts, D. M., 1994, Zero thickness interface elements - Numerical stability and application, Int. J. for Num. Anal. Meth. Geomech., 18, 10, 689–708.

[10] Elia, G., Amorosi, A., Chan, C., Kavvadas, M. J., 2010, Fully coupled dynamic analysis of an earth dam, Geotechnique, 61, 7, 549-563.

[11] Gazetas, G. 1987, Seismic response of earth dams: some recent developments, Soil Dyn. and Earthq. Engrg., 6, 1, 3–47.

[12] Hall, J. F., Chopra, A. K., 1982, Two-dimensional dynamic analysis of concrete gravity and embankment dams including hydrodynamic effects, Earthq. Engrg. and Struct. Dyn., 10, 2, 305-332.

[13] Kellezi, L. X., 2000, Local transmitting boundaries for transient elastic analysis, Soil Dyn. and Earthq. Engrg., 19, 7, 533-547.

[14] Kontoe, S., Zdravković, L., Potts. D.M., 2008, An assessment of time integration schemes for dynamic geotechnical problems, Comput. and Geotech., 2008, 35, 253-264.

[15] Kontoe, S., Zdravković, L., Potts. D. M., 2009, An assessment of the domain reduction method as an advanced boundary condition and some pitfalls in the use of conventional absorbing boundaries, Int. J. for Num. Anal. Meth. Geomech., 33, 309-330.

[16] Küçükarslan, S., Coşkun, S. B., Taşkin, B., 2005, Transient analysis of dam-reservoir interaction including the reservoir bottom effects, J. Fluids and Struct., 20, 1073-1084.

[17] Kuhlemeyer, R. L., Lysmer, J., 1973, Finite element method accuracy for wave propagation problems, J. Soil Mech. and Found. Div., ASCE, 99, 5, 421-427.

[18] Liu, P. L. F., 1986, Hydrodynamic pressures on rigid dams during earthquakes, J. Fluid Mech., 165, 131-145.

[19] Lysmer, J., Kuhlemeyer, R. L., 1969, Finite dynamic model for infinite media, J. Engrg. Mech. Div., ASCE, 95, 4, 859-877.

[20] Parrinello, F., Borino, G., 2007, Lagrangian finite element modelling of dam-fluid interaction: Accurate absorbing boundary conditions, Comput. and Struct., 85, 932-943.

[21] Potts, D. M., Zdravković, L., 1999, Finite element analysis in geotechnical engineering: Theory, Thomas Telford, London.

[22] Saini, S. S., Bettess, P., Zienkiewicz, O. C., 1978, Coupled hydrodynamic response of concrete gravity dams using finite and infinite elements, Earthq. Engrg. and Struct. Dyn., 6, 4, 363-374.

[23] Sarma, S. K., 1979, Stability analysis of embankments and slopes, J. Geotech. Engrg. Div., ASCE, 105, 12, 1511 - 1524.

[24] Sommerfeld, A. J. W., 1912, Die greensche funktion der schwingungsgleichung, Jahresbericht der Deutschen Methematiker-Vereinigung, 21, 309-353.

[25] Sommerfeld, A. J. W., 1949, Partial Differential Equations in Physics, Academic Press, New York.

[26] Terzaghi, K., 1950, Mechanics of landslides, Technical Report Engineering, Geology Volume, The Geological Survey of America.

[27] Tsai, C. S., Lee, G. C., Ketter, R. L., 1990, A semi-analytical method for time-domain analyses of dam-reservoir interactions, Int. J. for Num. Meth. Engrg., 29, 913-933.

[28] Von Estorff O., Antes H., 1991, On FEM-BEM coupling for fluid-structure interaction analyses in the time domain, Int. J. for Num. Meth. Engrg., 31, 6, 1151–1168.

[29] Westergaard, H. M., 1933, Water pressures on dams during earthquakes, Transactions, ASCE, 98, 1, 418-433.

[30] Wilson, E. L., Khalvati, M., 1983, Finite elements for the dynamic analysis of fluid-solid systems, Int. J. for Num. Meth. Engrg., 19, 11, 1657-1668.

[31] Woodward, P. K., Griffiths, D. V., 1996, Influence of viscous damping on the dynamic analysis of an earth dam using simple constitutive models, Comput. and Geotech., 19, 3, 245-263.

[32] Zangar, C. N., Haefeli, R. J., 1952, Electric analog indicates effect of horizontal earthquake shock on dams, Civil Engrg., 22, 4, 278-279.

[33] Zangar, C. N., 1953, Hydrodynamic pressures on dams due to horizontal earthquakes, Proc. Soc. Exp. Stress Anal., 10, 93-102.

A NOMENCLATURE

a maximum value of ramp acceleration load (= 1m/s^2)
a_o amplitude of harmonic acceleration load (= 1m/s^2)
$a(t)$ acceleration load time history
d maximum element size
f frequency of harmonic load
f_1 fundamental frequency of the reservoir
F_{dyn} total hydrodynamic force on the upstream reservoir face
F_{st} total hydrostatic force on the upstream reservoir face
g acceleration of gravity (= 9.81m/s^2)
G_w shear modulus of water
H height of the dam
K_d bulk modulus of the dam materials
K_w bulk modulus of water (= 2.2·10^{6}kPa)
L length of the reservoir
P_{dyn} hydrodynamic pressure at the base of the dam

r distance of the upstream reservoir boundary from the excitation source
t time
T thickness of the dam foundation
$\dot{u}$ velocity of water in the horizontal direction
$\ddot{u}_g$ horizontal ground acceleration
V_p p-wave velocity of water (= 1483m/s)
V_s shear wave velocity of the dam materials
W width of the dam crest
y vertical distance from the base of the dam
γ_w unit weight of water (= 9.81kN/m^3)
λ wavelength
λ_n nth wavelength
ρ mass density of water (= 1000kg/m^3)
σ normal stress on the upstream reservoir boundary
ω circular frequency of harmonic load
ω_1 fundamental circular freqency of the reservoir
Ω frequency ratio (= ω/ω_1)